ISSN 1070-3632, Russian Journal of General Chemistry, 2021, Vol. 91, No. 8, pp. 1572–1577. © Pleiades Publishing, Ltd., 2021.

Synthesis, Structure, DFT Calculations, and *In Silico* Toxic Potential of Ni(II), Zn(II), and Fe(II) Complexes with a Tridentate Schiff Base

N. Turan[a,*], E. Tanış[b], K. Buldurun[c], and N. Çolak[d]

[a] *Department of Chemistry, Faculty of Arts and Sciences, Muş Alparslan University, Muş, 49250 Turkey*
[b] *Department of Electrical Electronics Engineering, Faculty of Engineering and Architecture, Kırşehir Ahi Evran University, Kırşehir, 40100 Turkey*
[c] *Department of Food Processing, Technical Science Vocational School, Muş Alparslan University, Muş, 49250 Turkey*
[d] *Department of Chemistry, Faculty of Arts and Sciences, Hitit University, Çorum, 19100 Turkey*
**e-mail: nevintrn@hotmail.com; n.turan@alparslan.edu.tr*

Received March 29, 2021; revised May 5, 2021; accepted July 27, 2021

Abstract—The Schiff base ligand has been synthesized from 5-bromo-2-hydroxybenzaldehyde and ethyl 6-acetyl-2-amino-4,5,6,7-tetrahydrothieno[2,3-*c*]pyridine-3-carboxylate, and complexed with Ni(II), Zn(II), and Fe(II). Elemental analysis, spectral data and calculations on the DFT/UB3LYP/LANL2DZ level of the ligand and its metal(II) complexes have supported geometric and electronic characteristics of the compounds. Interactions of the products with 16 target proteins have been simulated. Kinetics stability, binding affinities (IC_{50}), and toxic potential (TP) of the ligand-protein complexes have been approached with the aid of molecular simulation. The ligand has been identified as a compound of low toxicity.

Keywords: DFT calculations, HOMO and LUMO levels, toxicology, Schiff base, metal complex

DOI: 10.1134/S107036322108020X

INTRODUCTION

Tridentate Schiff bases containing nitrogen, oxygen and sulfur donor atoms demonstrate efficient coordination with some metal ions [1]. DFT is a very strong computational tool for examination of molecular structures and spectroscopic properties of metal complexes [2–4]. Computational DFT methods are particularly efficient in identification of compounds toxicity with the help of global reactivity descriptors [5, 6]. Because of high cost and intensive labor, experimental toxicity studies could be somewhat limited. Therefore, over recent years, computational toxicology studies have been carried out extensively using various in silico techniques, that were quite compatible with the experimental studies [7–10]. In this study molecular docking led to accumulation of important data including molecule-protein free binding energies, toxicity and potential of development of new therapeutic agents [11, 12]. This way 16 proteins, including androgen (AR), estrogen alpha (ERα), estrogen beta (ERβ), mineralocorticoid (MR), liver X (LXR), glucocorticoid (GR), peroxisome proliferator-activated receptor (PPAR), thyroid alpha (TRα), thyroid beta (PR), and 10 nuclear receptors 1A1, 2C9, 2D6, 3A4 P450 enzyme family, aryl hydrocarbon receptor (AhR) and a potassium ion channel (hERG) have been singled out as the triggers of adverse effects.

Although Schiff bases and their metal complexes are widely reported, the physicochemical and toxic characteristics of (*E*)-ethyl-6-acetyl-2-(5-bromo-2-hydroxybenzylideneamino)-4,5,6,7-tetrahydrothieno-[2,3-*c*]pyridine-3-carboxylate (Fig. 1) and its Ni(II), Zn(II) and Fe(II) complexes (Fig. 2) have not been studied yet. The Schiff base ligand and its complexes were characterized by ^{1}H and ^{13}C NMR, FT-IR, UV-Vis, and LC-MS spectra, TGA, and magnetic susceptibility. Physicochemical properties were also figured out by the DFT/UB3LYP/LANL2DZ calculations. Structural, vibrational and electronic (molecular orbital energies and

Mulliken atomic charges) features were accumulated on the basis of 6-311G(d,p)+LanL2DZ, and those supported the experimental results.

EXPERIMENTAL

All chemicals and solvents used were purchased from Sigma-Aldrich and used without purification. The elemental analysis was carried out on a Leco CHNS-O 932 elemental analyzer. FT-IR spectra (KBr discs) were recorded on a Perkin Elmer-65 spectrophotometer. ^{1}H and ^{13}C NMR spectra were measured on a Brucker 300 and 75 MHz spectrometer using DMSO-d_6 as a solvent. Electronic spectra were recorded on a Shimadzu 1800 spectrophotometer. LC/MS mass spectra were measured on an AGILENT model 1100 MSD mass spectrometer. TGA was carried out on a Shimadzu DTG-60 AH thermal analyzer with the heating rate of 10°C/min under the atmosphere of N_2 at flow rate of 10 mL/min at 900°C. Magnetic susceptibilities were recorded at room temperature by the modified Gouy method and using $Hg[Co(SCN)_4]$ as a calibrate. Effective magnetic moments were calculated by the equation $\mu_{eff} = 2.84(X_M^{corrt}T)^{1/2}$. Melting points were determined by using a Stuart melting point apparatus.

(*E*)-Ethyl-6-acetyl-2-(5-bromo-2-hydroxybenzylideneamino)-4,5,6,7-tetrahydrothieno[2,3-*c*]pyridine-3-carboxlate. Ethyl 6-acetyl-2-amino-4,5,6,7-tetrahydrothieno[2,3-*c*]pyridine-3-carboxylate (1.33 g, 5.0 mmol) was dissolved in hot ethanol (30 mL) and added to the equimolar amount of 5-bromo-2-hydroxybenzaldehyde (1.00 g, 5.0 mmol) in ethanol (20 mL) upon stirring. The mixture was refluxed for 5 h and then cooled down to room temperature. The yellow precipitated product was isolated, washed with cold ethanol and recrystallized from ether–ethanol (2 : 1). Yield 86%, mp 225°C. FT-IR spectrum, ν, cm^{-1}: 3388 (OH), 3184 (C–H_{Ar}), 2982, 2907 (C–H_{Alip}), 1696, 1636 (C=O), 1601 (CH=N), 1543, 1482 (Ar-C=C), 1189 (C–O), 783 (C–S–C). ^{1}H NMR spectrum, δ, ppm: 12.96 s (1H, Ar–O*H*), 8.43 s (1H, C*H*=N), 7.20–6.80 m (3H, Ar–C*H*), 4.31 m (2H, OCH_2CH$_3$), 2.91–2.64 m (6H, pyridine-CH_2), 3.49 s (3H, NCOCH_3), 1.33 t (3H, OCH$_2$CH_3). ^{13}C NMR spectrum, δ_C, ppm: 14.4, 26.8, 28.8–52.3, 60.6, 117.6–134.5, 132.2–153.7, 159.3, 161.1. Found, %: C 50.55; H 4.20; N 6.20; S 7.15. $C_{19}H_{19}BrN_2O_4S$. Calculated, %: C 50.51; H 4.21; N 6.20; S 7.10. MS: *m/z*: 453.02 $[M + 2H]^+$.

Synthesis of the complexes. The Schiff base ligand (0.90 g, 0.2 mmol) was dissolved in 15 mL of ethanol, then ethanol solution (15 mL) of one of $NiCl_2·6H_2O$ (0.48 g, 0.2 mmol), $ZnCl_2$ (0.27 g, 0.2 mmol) or $FeCl_2·4H_2O$ (0.39 g, 0.2 mmol) was slowly added to the reaction mixture which was refluxed for 6 h. The reaction mixture was cooled down to room temperature and concentrated in vacuum to precipitate a colored solid, which was isolated by vacuum filtration and washed by diethyl ether. The crude product was recrystallized from ethanol, washed with diethyl ether and dried over $CaCl_2$ in vacuum.

Ni(II) complex. Brown solid, yield 80%, mp >260°C. FT-IR spectrum, ν, cm^{-1}: 3493, 3321 (OH), 3199 (C–H_{Ar}), 2937 (C–H_{Alip}), 1695, 1645 (C=O), 1611 (CH=N), 1543 (Ar-C=C), 1192 (C–O), 784 (C–S–C), 472 (M–O), 569 (M–N). Found, %: C 35.98; H 4.40; N 4.38; S 5.04. $C_{19}H_{28}BrN_2O_9SClNi$. Calculated, %: C 35.97; H 4.41; N 4.41; S 5.05. *M* 634.29. UV-Vis spectrum, λ_{max}, nm: 261, 296, 332, 501, 710. MS: *m/z*: 633.06 $[M - H]^+$. μ_{eff} (B.M.): 3.03.

Zn(II) complex. Orange solid, yield 76%, mp >260°C. FT-IR spectrum, ν, cm^{-1}: 3514, 3434 (OH), 3051 (C–H_{Ar}), 2982, 2933 (C–H_{Alip}), 1697, 1648 (C=O), 1598 (CH=N), 1545 (Ar-C=C), 1184 (C–O), 783 (C–S–C), 472 (M–O), 584, 542 (M–N). Found, %: C 35.62; H 4.30; N 4.33; S 4.99. $C_{19}H_{28}BrN_2O_9SClZn$. Calculated, %: C 35.60; H 4.36; N 4.36; S 5.01. *M* 640.98. UV-Vis spectra, λ_{max}, nm: 206, 295, 392, 410, 483, 600. MS: *m/z*: 639.98 (calc), 640.00 (found) $[M - H]^+$. μ_{eff} (B.M.): Dia.

Fe(II) complex. Brown solid, yield 78%, mp >260°C. FT-IR spectrum, ν, cm^{-1}: 3491, 3411 (OH), 3051 (C–H_{Ar}), 2975, 2903 (C–H_{Alip}), 1696, 1647 (C=O), 1595 (CH=N), 1566, 1519 (Ar-C=C), 1180 (C–O), 784 (C–S–C), 472, 495 (M–O), 586, 525 (M–N). Found, %: C 35.14; H 4.62; N 4.30; S 4.94. $C_{19}H_{30}BrN_2O_{10}SClFe$. Calculated, %: C 35.13; H 4.61; N 4.31; S 4.93. UV-Vis spectrum, λ_{max}, nm: 206, 291, 399, 411, 499. MS: *m/z*: 648.98 $[M - H]^+$. μ_{eff} (B.M.): 4.30.

Computational details. All calculations for the ligand and its complexes were carried out using the Gaussian 09 package program [13]. The results were visualized with the help of the GaussView5 program [14]. The primarily optimization was based on DFT/UB3LYP method with the 6-311G(d,p) basis set for C, H, O, N, and Cl atoms and the LanL2DZ basis set for Fe, Ni, and Zn atoms. The harmonic frequencies were multiplied by the scaling factor [15] to approximate the calculated vibration frequencies to the experimental vibration frequencies. To verify the electronic transitions, HOMOs and LUMOs

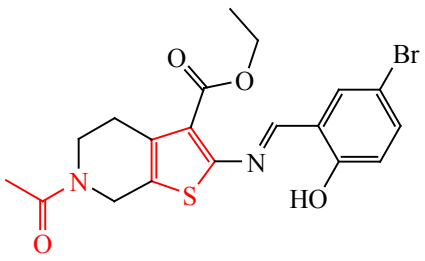

Fig. 1. Chemical structure of the ligand (*E*)-ethyl-6-acetyl-2-(5-bromo-2-hydroxybenzylideneamino)-4,5,6,7-tetrahydrothieno[2,3-*c*]pyridine-3-carboxlate.

were approached using the optimized molecular structures in chloroform. The atomic charge distributions of the ligand and complexes were determined by Mulliken population analysis using the DFT/UB3LYP/Lanl2DZ basis set. The toxic potential of the ligand was determined from 16 target protein-ligand interactions using the VirtualToxLab software.

RESULTS AND DISCUSSION

The ligand and its complexes were stable at room temperature. Elemental analysis, FT-IR, ^{1}H, and ^{13}C NMR, and mass spectra supported the proposed structures of the synthesized compounds.

In FT-IR spectra of the complexes the shift of CH=N stretching vibrations to lower or higher wavenumbers indicated coordination of the ligand via the azomethine nitrogen [16]. Stretching vibrations of the C=O group of the ligand recorded at 1636 cm^{-1} were shifted to 1645, 1648, 1647 cm^{-1} in the spectra of Ni(II), Zn(II), and Fe(II) complexes, respectively, which confirmed coordination of the oxygen atom with the metal ions [17]. The C=O stretching bands were calculated for the ligand at 1667 cm^{-1}, and for Fe(II) at 1612 cm^{-1}, for Zn(II) at 1607 cm^{-1}, and for Ni(II) at 1632. The phenolic OH stretching band at 3388 cm^{-1} of the ligand disappeared upon complexation. The free ligand phenolic C–O band was shifted to lower and higher values by 3–9 cm^{-1} upon complexation indicating its coordination to the metal ions [18]. The new bands observed at 584–525 and 495–472 cm^{-1} were assigned to M–N and M–O, respectively [19]. The significant shifts of the CH=N, phenolic OH and C=O groups bands suggested the tridentate ONO donor ligand character in the complexes.

The shifts of the bands in UV-Vis spectra were associated with the intra-molecular transitions of the $\pi \rightarrow \pi^*$ and $n \rightarrow \pi^*$ types, and could be attributed to involvement of N atoms of the ligand in the coordination process [20]. Electronic spectrum of Ni(II) complex was characterized by the bands at 501 and 710 nm related to $^{3}A_{2g}(F) \rightarrow {}^{3}T_{1g}(P)$ and $^{3}A_{2g}(F) \rightarrow {}^{3}T_{1g}(P)$ transitions, respectively, suggesting its octahedral geometry [21]. The magnetic moment value of Ni(II) complex (3.03 B.M.) pointed out existence of two unpaired electrons in the octahedral structure [22]. The Fe(II) complex exhibited the bands at 399 and 499 nm, that were ascribed to the metal-ligand charge and $^{4}T_{1g} \rightarrow {}^{4}T_{2g}(F)$ transitions, respectively. Magnetic moment of the Fe(II) complex (4.30 B.M.) was consistent with its octahedral geometry [23]. The Zn(II) complex bands recorded at 392, 410, and 483 nm were correlated with the $n \rightarrow \pi^*$ transition (the first band) and the S → Zn charge transfer [24, 25].

The TGA profiles of the complexes were similar and exhibited three main stages. The first one was in the range of 50–300°C and related to the loss of hydrated and coordinated water. The second step was recorded in the range of 350–800°C and corresponded to the mass loss of organic moiety. At the third step the metal complexes

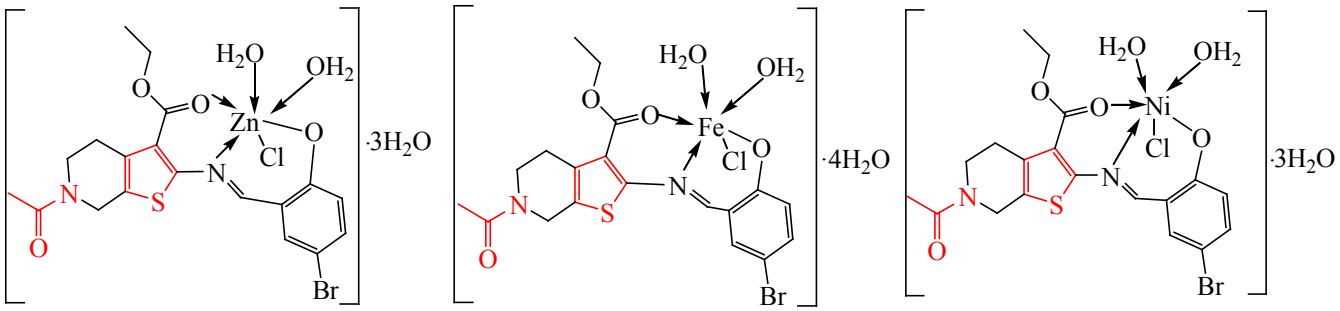

Fig. 2. The proposed structures of the synthesized metal complexes.

Table 1. Selected calculated bond lengths and angles for the ligand and its complexes

Bond, angle	Ligand	Fe(II) complex	Ni(II) complex	Zn(II) complex	Bond, angle	Ligand	Fe(II) complex	Ni(II) complex	Zn(II) complex
DFT/UB3LYP/LANL2DZ									
Bond	*d*, Å				Bond	*d*, Å			
C^1–C^2	1.34	1.34	1.37	1.37	C^{12}–N^{25}	1.47	1.47	1.47	1.47
C^3–C^7	1.54	1.35	1.35	1.34	N^{25}–C^{15}	1.47	1.47	1.47	1.47
C^8–S^{26}	1.77	1.76	1.76	1.76	C^{17}–O^{22}	1.26	1.28	1.43	1.28
C^8–C^9	1.53	1.34	1.34	1.34	C^{15}–O^{23}	1.43	1.43	1.28	1.43
C^7–N^{24}	1.36	1.48	1.48	1.47	N^{25}–C^{13}	1.29	1.29	1.29	1.29
C^7–H^{37}	1.07	1.07	1.07	1.07	C^{15}–C^{16}	1.54	1.53	1.53	1.53
C^8–N^{24}	1.48	1.35	1.35	1.35	N^{24}–M	–	1.40	1.40	1.40
C^6–H^{36}	1.07	1.07	1.07	1.07	C^1–Br^{27}	1.91	1.91	1.91	1.91
C^{10}–C^{11}	1.36	1.47	1.47	1.47	Cl^{31}–M	–	1.39	1.39	1.40
C^{11}–S^{26}	1.78	1.61	1.61	1.61					
Angles	φ, deg				Angles	φ, deg			
$C^8S^{26}C^{11}$	91.55	89.76	89.76	89.76	$C^1C^2C^3$	112.81	114.12	114.12	114.12
$C^7N^{24}C^8$	114.94	113.61	113.61	113.61	$N^{24}MO^{21}$	120.70	126.44	126.44	126.44
$N^{25}C^{15}O^{23}$	121.84	120.75	120.75	120.75					

decomposed gradually with formation of metal oxides above 600°C.

Structural analysis. Sample of optimized geometric structures of the ligand and Fe(II) complex are presented in Fig. 3. The selected bond lengths and bond angles of these structures are listed in Table 1. The optimized structures were octahedral, stabilized by two water molecules with N, O and Cl atoms around the metal atoms. According to the accumulated data (Table 1) the bond lengths of the metal atoms with the surrounding atoms in all compounds did not change. The length of the C=N bond in the imine group was prolonged when it coordinated to a metal center, and additionally, separation of the phenolic OH group caused reduction in the C–C bond lengths between both the phenolic C–O and the imine group and the phenyl ring [26–29].

Electronic properties. The calculated energy gap (E_g) between HOMO and LUMO was calculated to be 2.58 eV for the ligand, 2.92 eV for Fe(II), 3.09 eV for Zn(II), and 2.99 eV for Ni(II) complexes. The above data indicated that conductivity and reactivity of the complexes were increasing in the order of ligand > Fe(II) > Ni(II) > Zn(II).

Atomic charge distributions and dipole moments. The individual atomic charge values obtained from the Mulliken population demonstrated that the charges of S

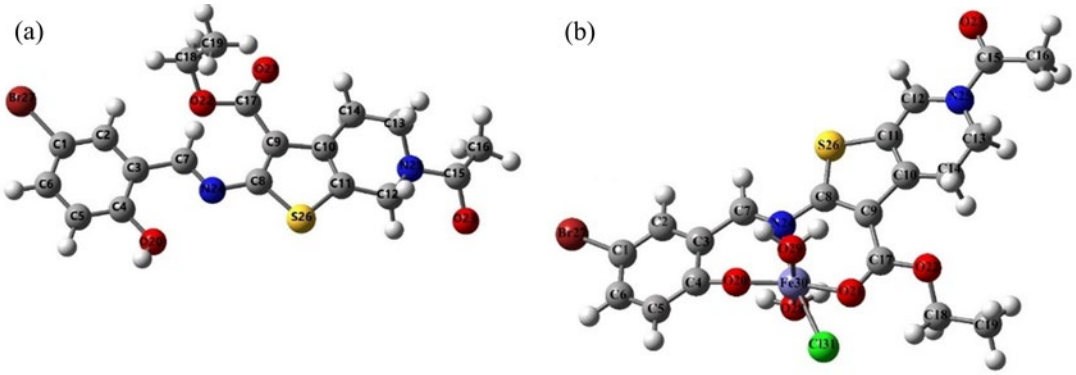

Fig. 3. The optimized structures of the (a) ligand and (b) Fe(II) complex.

Table 2. Binding affinities (IC_{50} nanomolar) of the ligand against all 16 target proteins in the *VirtualToxLab*

Proteins	Ligand
AR	Not binding
AhR	0.001730
CYP1A2	Not binding
CYP2C9	Not binding
CYP2D6	Not bonding
CYP3A4	Not binding
ERα	Not binding
ERβ	Not binding
GR	0.068700
hERG	0.082300
LXR	0.008670
MR	Not binding
PPARγ	0.003610
PR	0.046000
TRα	0.052000
TRβ	0.023200

atoms were 0.345 *e* for the ligand, 0.404 *e* for the Fe(II) complex, 0.385 *e* for the Zn(II) complex and 0.416 *e* for the Ni(II) complex. Similarly, charge of the atom N^{22} was –0.295 *e* for the ligand, –0.690 *e* for the Fe(II) complex, –0.722 *e* for the Zn(II) complex, and –0.664 *e* for the Ni(II) complex. The above data indicated that there was electrons transfer from the metal cations to the anions and ring atoms.

In silico prediction of the IC_{50} and TP of the ligand. In this study, we simulated interactions of the optimized ligand molecule using the DFT/B3LYP/6-311G(d,p) basis set with 16 proteins identified in *VirtualToxLab* and obtained binding affinity (IC_{50}) and total toxic potential (TP) of each protein to the ligand. The value of TP varied from 0.0 to 1.0 as TP ≤ 0.3 (low), 0.3 < TP ≤ 0.6 (moderate), 0.6 < TP ≤ 0.8 (high) and TP > 0.8 (extreme). The total TP value was calculated as 0.369 (low). The calculated binding affinity values for the 16 target proteins in this platform for the ligand are presented in Table 2. The table also defines the "not binding" bond affinity>100 μM. The highest affinities AhR (0.001730 nM) and PPARγ (0.003610 nM) were determined. Both ligand-protein complexes were stabilized by a weak H-bond with the terminal O atoms, that were electron donors of the ligand.

CONCLUSIONS

The synthesized Schiff base and its complexes have been characterized by IR, UV-Vis, NMR, and LC-MS spectroscopy, TGA, magnetic susceptibility, and elemental analysis. The six-coordinated geometry has been assigned to Zn(II), Ni(II), and Fe(II) complexes. The detailed analysis of the synthesized molecules has been performed using quantum chemical calculations. The calculations and experimental data match well. The ligand and its complexes have been characterized by negative HOMO and LUMO energy levels, indicating stability of the compounds. Probability of electron transfer from the metal cations to the anions and ring atoms is based on the Mulliken analysis. The binding affinity values have been calculated using the *VirtualToxLab* software and indicated low toxicity of the ligand (toxic potential value of 0.369).

CONFLICT OF INTEREST

No conflict of interest was declared by the authors.

REFERENCES

1. Mayer, P., Potgieter, K.C., and Gerber, T.I.A., *Polyhedron,* 2010, vol. 29, p. 1423. https://doi.org/10.1016/j.poly.2010.01.013
2. Dikmen, G. and Hür, H., *Chem. Phys. Lett.,* 2019, vol. 716, p. 49. https://doi.org/10.1016/j.cplett.2018.12.018
3. Sayın, K., Kariper, S.E., Taştan, M., Sayın, T.A., and Karakaş, D., *J. Mol. Struct.,* 2019, vol. 1176, p. 478. https://doi.org/10.1016/j.molstruc.2018.08.103
4. Li, J., Ren, G., Zhang, Y., Yang, M., and Ma, H., *Polyhedron,* 2019, vol. 157, p. 163. https://doi.org/10.1016/j.poly.2018.09.052
5. Çankaya, N., Tanış, E., Gülbaş, H.E., and Bulut, N., *Polym. Bull.,* 2019, vol. 76, p. 3297. https://doi.org/10.1007/s00289-018-2543-3
6. De Proft, F. and Geerlings, P., *Chem. Rev.,* 2001, vol. 101, p. 1451. https://doi.org/10.1021/cr9903205
7. Singh, R., Bhardwaj, V., Das, P., and Purohit, R., *J. Biomol. Struct. Dyn.,* 2020, vol. 38 p. 5126. https://doi.org/10.1080/07391102.2019.1696709
8. Bhardwaj, V.K., Singh, R., Sharma, J., Das P., and Purphit, R., *Comput Meth. Prog. Bio.,* 2020, vol. 194, p. 105494. https://doi.org/10.1016/j.cmpb.2020.105494
9. Bhardwaj, V.K. and Purohit, R., *Genomics,* 2020, vol. 112, p. 3729.

https://doi.org/10.1016/j.ygeno.2020.04.023

10. Singh, R., Bhardwaj, V.K., Sharma, J., Das P., and Purohit R., *Genomics,* 2021, vol. 113, p. 707. https://doi.org/10.1016/j.ygeno.2020.10.001
11. Vedani, A. and Smiesko, M., *Altern. Lab. Anim.,* 2009, vol. 37, p. 477. https://doi.org/10.1177/026119290903700506
12. Vedani, A., Dobler, M., Hu, Z., and Smieško, M., *Toxicol. Lett.,* 2015, vol. 232, p. 519. https://doi.org/10.1016/j.toxlet.2014.09.004
13. Frisch, M.J., Trucks, G.W., Schlegel, H.B., Scuseria, G.E., Robb, M.A., Cheeseman, J.R., Scalmani, G., Barone, V., Mennucci, B., Petersson, G.A., Nakatsuji, H., Caricato, M., Li, X., Hratchian, H.P., Izmaylov, A.F., Bloino, J., Zheng, G., Sonnenberg, J.L., Hada, M., Ehara, M., Toyota, K., Fukuda, R., Hasegawa, J., Ishida, M., Nakajima, T., Honda, Y., Kitao, O., Nakai, H., Vreven, T., Montgomery, Jr.J.A., Peralta, J.E., Ogliaro, F., Bearpark, M., Heyd, J.J., Brothers, E., Kudin, K.N., Staroverov, V.N., Kobayashi, R., Normand, J., Raghavachari, K., Rendell, A., Burant, J.C., Iyengar, S.S., Tomasi, J., Cossi, M., Rega, N., Millam, J.M., Klene, M., Knox, J.E., Cross, J.B., Bakken, V., Adamo, C., Jaramillo, J., Gomperts, R., Stratmann, R.E., Yazyev, O., Austin, A.J., Cammi, R., Pomelli, C., Ochterski, J.W., Martin, R.L., Morokuma, K., Zakrzewski, V.G., Voth, G.A., Salvador, P., Dannenberg, J.J., Dapprich, S., Daniels, A.D., Farkas, O., Foresman, J.B., Ortiz, J.V., Cioslowski, J., and Fox, D.J., Gaussian 09, Revision A.1, Gaussian, Inc., Wallingford CT, 2009 *Gaussian 09*, Revision A.1. Gaussian, Inc., Wallingford, 2009.
14. GaussView 5.0 Gaussian Inc. Wallingford, CT, USA, 2009.
15. http://cccbd b.nist.gov/vsfx.asp
16. Chaudhary, N.K. and Mishra, P., *J. Saudi. Chem. Soc.,* 2018, vol. 22, p. 601. https://doi.org/10.1016/j.jscs.2017.10.003
17. Mohanana, K. and Devi, S.N., *Russ. J. Coord. Chem.,* 2006, vol. 8, p. 600. https://doi.org/10.1134/S1070328406080124
18. Shukla, S.N., Gaur, P., Raida, M.L., and Chaurasia, B., *J. Mol. Struct.,* 2020, vol. 1202, 127362. https://doi.org/10.1016/j.molstruc.2019.127362
19. Chang, H.Q., Jia, L., Xu, J., Wu, W.N., Zhu, T.F., Chen, R.H., Ma, T.L., Wang, Y., and Xu, Z.Q., *Transit. Met. Chem.,* 2015, vol. 40, p. 485. https://doi.org/10.1007/s11243-015-9938-x
20. Tas, E., Kilic, A., Durgun, M., Küpecik, L., Yilmaz, I., and Arslan, S., *Spectrochim. Acta A,* 2010, vol. 75, p. 811. https://doi.org/10.1016/j.saa.2009.12.002
21. El-Shafiy, H.F., Saif, M., Mashaly, M.M., Abdel Halim, S., Eid, M.F., Nabeel, A.I., and Fouad, R., *J. Mol. Struct.,* 2017, vol. 1147, p. 452. https://doi.org/10.1016/j.molstruc.2017.06.121
22. Anacona, J. and Santaella, J., *Spectrochim. Acta A,* 2013, vol. 115, p. 800. https://doi.org/10.1016/j.saa.2013.06.107
23. Abdel-Rahman, L.H., Ismail, N.M., Ismael, M., Abu-Dief, A.M., and Ahmed, E.A.H., *J. Mol. Struct.,* 2017, vol. 1134, p. 851. https://doi.org/10.1016/j.molstruc.2017.01.036
24. Kumar, S., Hansda, A., Chandra, A., Kumar, A., Kumar, M., Sithambaresan, M., Faizi, M.S.H., Kumar, V., and John, R.P., *Polyhedron,* 2017, vol. 134, p. 11. https://doi.org/10.1016/j.poly.2017.05.055
25. Manjunath, M., Kulkarni, A.D., Bagihalli, G.B., Malladi, S., and Patil, S.A., *J. Mol. Struct.,* 2017, vol. 1127, p. 314. https://doi.org/10.1016/j.molstruc.2016.07.123
26. Uh, Y.S., Zhang, H., Vogels, C.M., Decken, A., and Westcott, S.A., *Bull. Kor. Chem. Soc.,* 2004, vol. 25, p. 986. https://doi.org/10.5012/bkcs.2004.25.7.986
27. Akbari, A. and Alinia, Z., *Turk J. Chem.,* 2013, vol. 37, p. 867. https://doi.org/10.3906/kim-1207-74
28. Mariappan, M., Suenaga, M., Mukhopadhyay, A., and Maiya, B.G., *Inorg. Chim. Acta,* 2012, vol. 390, p. 95. https://doi.org/10.1016/j.ica.2012.04.016
29. Blackburn, O.A., Coe, B.J., Fielden, J., Helliwell, M., McDouall, J.J.W., and Hutchings, M.G., *Inorg. Chem.,* 2010, vol. 49, p. 9136. https://doi.org/10.1021/ic1000842